



## The Non-linear dynamics and Non-linear bias for galaxy formation in Redshift Space

El Yamani Diaf<sup>1,2</sup>

*1. Equipe de Physique Theorique et Simulation (EPTE)*

*Departement des Sciences Exactes, Faculte Pluridisciplinaire de Nador*

*Universite Mohamed 1, B.P 300, Selouane, Nador, Morocco*

*2. Groupement de Physique des Hautes Energies, Siege focal, Lab/UFR-HEP, Rabat, Morocco.*

*eldiaf@gmail.com*

### Abstract

We measure the  $\beta$  parameter using the quadrupole to monopole ratio from power spectrum and compare with the true asymptotic value  $\beta \simeq \frac{\Omega_b^{0.6}}{b}$  we get that there is an agreement in the values of these two quantities. In addition, we have studied the non-linear dynamics and non-linear bias of galaxies. We done it in two ways: Theoretically and using N-body simulation. We find excellent agreement in both theory and GIF simulation. In this case, we can see clearly how the non-linear effect, redshift distortion and non-linear bias evolves in real and redshift space.

**keywords:** cosmology: theory - galaxies: redshift distortion - galaxies: Non-linear (bias & dynamics), large-scale structure of Universe- galaxies: GIF simulation and theory.

### I. INTRODUCTION

A spherical over density appears distorted by peculiar velocities when observed in Redshift Space. On large (linear) scale the over density appears squashed along the line of sight, while on small (non-linear) scales fingers-of-God appear where the distortions at projected separations  $\simeq 0.2h^{-1}\text{Mpc}$ . The over density is far from the observer, and the distortions are effectively plane-parallel. For the over density is near the observer, and the large scale distortions appear kindly-shaped, while the finger-of-God is sharper on the end pointing at the observer. The observer shares the infall motion towards the overdensity. A similar diagram appears in Kaiser's formula (1987). For the universe that obeys the cosmological principle, the clustering of galaxies is statically isotropic. But in galaxies redshift surveys the distances to galaxies are inferred from redshift, making line of sight a preferred direction.

On small scales, the non linear scales anisotropy in the power spectrum is dominated by galaxy velocity dispersion in virialized clusters. In the linear regime of gravitational instability models, the anisotropy of clustering takes a very simple form in Fourier space, as shown by (Kaiser 1987; McGill 1990). The strength of an individual plane wave is amplified by a factor that depends on the angle between the wavevector and the line of sight,  $\delta_k^s = \delta_k^r (1 + \beta \mu_{kl}^2)$  where  $\delta_k^r$  and  $\delta_k^s$  denote the Fourier amplitudes in real and redshift space, respectively, and  $\mu_{kl}$  is the cosine of the angle between the wavevector,

---

<sup>0</sup>© a GNPHE publication 2007, *ajmp@fsr.ac.ma*

$k$ , and the line of sight,  $l$ . The degree of amplification is controlled by  $\beta \equiv \Omega_0^{0.6}/b$ , where  $\Omega_0^{0.6}$  is the logarithmic derivative of fluctuation growth rate (Peebles 1980, section 14), and  $b$  is the bias factor, and assumed constant of proportionality between galaxy and mass fluctuations.

The aim of this paper is to measure the  $\beta$  parameter using the power spectrum quadrupole to monopole ratio and compare the power spectrum of galaxies and matter in both real and redshift space in the linear regime. We have chosen to study the evolution of galaxies in a representative variant of CDM-type models: The low matter density, flat, CDM model with cosmological constant ( $\Lambda$ CDM):  $\Omega_0=1-\Omega_\Lambda=0.3$ ,  $h=0.7$ , where  $\Omega_0$  and  $\Omega_\Lambda$  are present-day matter and vacuum densities, and  $h$  is the dimensionless Hubble constant defined as  $H_0=100h\text{km/s/Mpc}$ . This model is arguably the most successful model in matching a variety of existing data. Observations of galaxy cluster evolution Eke et al. (1996), baryons fraction in clusters Evrad (1997), and high-redshift supernovae (e.g., Falco et al. 1997; Salaris & Cassisi 1998; Madore et al. 1999) tend to converge on the values of  $h \simeq 0.6-0.7$ .

Our second study is to see the non-linear effect, redshift distortion and non-linear bias in real and redshift space. We focus to see the result of power spectrum in redshift space using calculation formally done by Heavens (1998) with small change and applied them to GIF data. The plan of this paper is as follows: In § 2 we discussed the linear theory for the power spectrum which led to estimated the value of  $\beta$  for galaxies in redshift space. The value of  $\beta$  in this case is calculated from the quadrupole to monopole ratio. This theory will be applied to analysis of the data from the GIF N-body simulation. In § 3 we investigated the effect of non-linearities, redshist distortions and non-linear bias on the power spectrum of galaxies in redshift space. In § 4, we give a summary and discussion.

## II. LINEAR THEORY STUDIES OF POWER SPECTRUM

It is possible to estimate  $\beta$  simply by analyzing the redshift space distortions, or, more specifically, by measuring the anisotropy of galaxy clustering in redshift space. Kaiser (1987) showed that, in the linear regime, the redshift space galaxy power spectrum,  $P_g^s(k, \mu)$  is related to the real space galaxy power spectrum,  $P_g^r(k)$  by

$$P_g^s(k, \mu) = (1 + \beta\mu^2)^2 P_g^r(k) \quad (2.1)$$

In real space, the  $\beta$  parameter will be calculated from the relation  $\beta \equiv \Omega_0^{0.6}/b$ , such that the bias parameter  $b$  obtained from the square root of the ration of power spectrum of galaxies to the power spectrum of matter in real space,  $b = \sqrt{\frac{P_g^r(k)}{P_s^r(k)}}$ . The application of this relation leads to find that  $\beta \sim 0.40 \pm 0.06$  which very closed to the true asymptotic value  $\Omega_0^{0.6}/(b = 1) \sim 0.48$  which will be comparated to the results of the new one of Jeremy L. *et.al* 2005.

### A. $\beta$ estimator from quadrupole to monopole ratio

Let us characterized the redshift-space power spectrum in terms of multipole moments define by the decomposition of  $P^s(k, \mu)$  into Legendre polynomials, hereafter denoted  $\mathcal{P}_\ell(\mu)$ ,

$$P^s(k, \mu) = \sum_{\ell=0}^{\infty} P_\ell^s(k) \mathcal{P}_\ell(\mu). \quad (2.2)$$

such that the multipole moments,  $P_\ell^s(k)$ , can be computed by the inversion formula

$$P_\ell^s(k) \equiv \frac{2\ell+1}{2} \int_{-1}^{+1} d\mu P^s(k, \mu) \mathcal{P}_\ell(\mu). \quad (2.3)$$

The first three even Legendre polynomials are:  $\mathcal{P}_0(\mu) = 1$ ,  $\mathcal{P}_2(\mu) = \frac{(3\mu^2-1)}{2}$ ,  $\mathcal{P}_4(\mu) = \frac{(35\mu^4-30\mu^2+3)}{8}$ .

In the linear theory,  $P^s(k, \mu)$  has the simple angular dependence of equation  $\delta_k^s = \delta_k^r(1 + \beta\mu_{kl}^2)$ , which is characterized completely by its monopole, quadrupole. The non-vanishing moments can be obtained easily by direct integration:

$$\begin{aligned} P_0^s(k) &= (1 + \frac{2}{3}\beta + \frac{1}{5}\beta^2)P^r(k) \\ P_2^s(k) &= (\frac{4}{3}\beta + \frac{4}{7}\beta^2)P^r(k) \\ P_4^s(k) &= (\frac{8}{35}\beta^2)P^r(k) \end{aligned} \quad (2.4)$$

$P_\ell^s(k) = 0$  for  $\ell \neq 0, 2$  or  $4$  and  $P^r(k)$  is the power spectrum in real space.

When clustering (halo of galaxies) is non-linear, one can still perform a multipole decomposition of the power spectrum as in equation (2), but the low-order moments will depart from the values in equation (4). In particular, the finger-of-God distortion reverses the sign of the quadrupole term on small scales, because it weakens fluctuations along the line of sight instead of amplifying them. If we have measured  $P^s(k, \mu)$  on large scales and decomposed it into multipole moments, then we can estimate  $\beta$  from the ratio of the quadrupole term to the monopole term. The linear theory prediction, which follows directly from (4), is

$$\frac{P_2^s}{P_0^s} = R(\beta) \equiv \frac{\frac{4}{3}\beta + \frac{4}{7}\beta^2}{1 + \frac{2}{3}\beta + \frac{1}{5}\beta^2} \quad (2.5)$$

The application of the quadrupole to monopole power spectrum ratio to the measurement of the the  $\beta$  parameter from the GIF data analysis, is shown in Fig. 1. This preliminary application the value  $\beta$  as:  $\beta \sim 0.2 - 0.4$  at wavenumbers  $k \simeq 0.14 - 0.22 h Mpc^{-1}$  (i.e.  $\lambda \simeq 30 - 45 h^{-1} Mpc$ ). The linear value of  $\beta$  parameter is very close to the true value of the simulation  $\beta = 0.48$ .

However, non-linearity in the density field produces distortions in an opposite sense to the linear theory predictions, leading to systematically lower estimates of  $\beta$  even on scales as large as  $90 h^{-1} Mpc$ . The modeling of the non-linearities accurately is needed in order to estimate  $\beta$  using currently available redshift surveys. Cole et al (1995) estimated  $\beta$  from  $\frac{P_2(k)}{P_0(k)}$  by assuming an exponential velocity distribution model, in which galaxies have uncorrelated small-scale peculiar velocities drawn from an exponential distribution in addition to their linear theory velocities. Applying this method to the IRAS 1.2 Jy redshift survey, they found  $\beta_{IRAS} = 0.52 \pm 0.13$ . This result agrees with our case such that at small scales ( $k$  small scales =  $\lambda$  larger), we found for matter ( $\Lambda$  CDM) the parameter is  $\beta \simeq 0.5$  at wavelength  $\lambda \simeq 95 h^{-1} Mpc$ . Other studies done by Fisher & Nusser (1996), modeled the non-linearity in  $\frac{P_2(k)}{P_0(k)}$  by using the Zel'dovich approximation, thus assuming that the scale dependence in this ratio is caused by coherent, rather than random, non-linear motions. They found  $\beta_{IRAS} = 0.6 \pm 0.2$  which is also close to our result such that  $\beta = 0.5$  for  $\lambda = 100 h^{-1} Mpc$ . Hatton & Cole (1999) proposed and tested an empirical model for the non-linearity in  $\frac{P_2(k)}{P_0(k)}$  by examining the scale dependance of this ratio in large number of N-body simulation while the analysis of 2dFGRS presented by Hawking *et al.* (2003), yielding  $\beta = 0.49 \pm 0.09$ , updating the earlier 2dFGRS analysis of Peacock *et al.* (2001). This model is more general and very close to the GIF simulation we analyzed in our studies than the previous cases cited before (IRAS 1.2 Jy). Their model for the N-body simulation is based on fully non-linear N-body data. The large scale structure of this model (for example the large boxlength as  $141.30 h^{-1} Mpc$  for  $\Lambda$ CDM cosmology) will be given the result of  $\beta$  parameter much better, although even the non-linearity will be important.

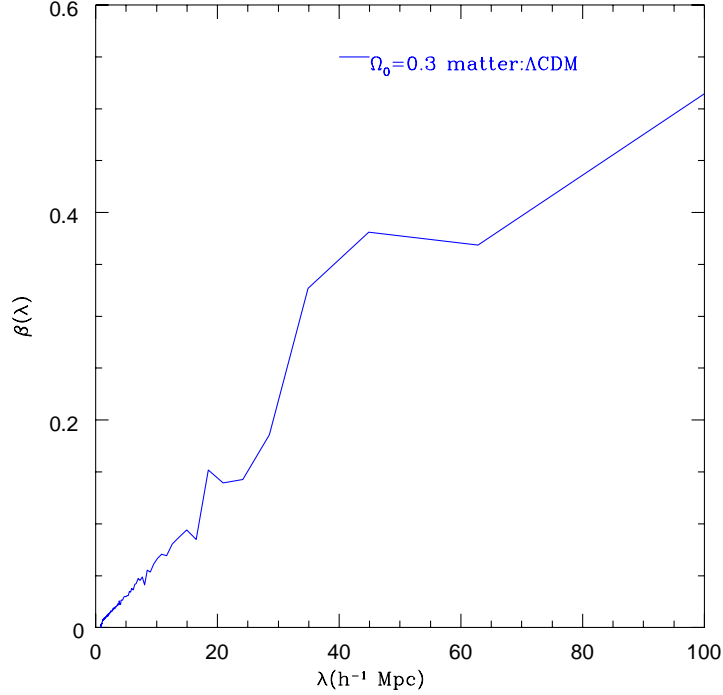


FIG. 1. The  $\beta$  parameter values calculated from the quadrupole to monopole power spectrum. Here for the small value of wavevector (linear case) the value of  $\beta$  is closed to the true value ( $\beta = 0.48$ ), but when the wavevector is smaller (non-linear case) the  $\beta$  parameter becomes larger, see text.

### III. NON-LINEAR STUDIES OF POWER SPECTRUM

#### A. Non-linear dynamics

Let  $r$  and  $s$  be the real and redshift-space coordinates, with the observer at the origin. We define  $\rho_r(r)$  and  $\rho_s(s)$  to be the density field in real and redshift space. The mean density is spatially dependent, because of selection effects; we define the selection functions as  $\Phi_r(r)$  and  $\Phi_s(s)$ . The overdensity in redshift space is defined by  $1 + \delta_s(s) \equiv \rho_s(s)/\Phi_s(s)$ , and similarly for the real-space overdensity  $\delta_r$ .

The coordinate transform from real space to redshift space is (Kaiser 1987)

$$s(r) = r \left[ 1 + \frac{U(r) - U(0)}{r} \right]. \quad (3.1)$$

where  $U(r) \equiv v \hat{r} = v \frac{\vec{r}}{r}$ . From conservation of mass,

$$\rho_r(r) d^3 r = \rho_s(s) d^3 s. \quad (3.2)$$

we get

$$[1 + \delta_g(s)] \phi_s(s) = \frac{[1 + \delta_r(r)] \phi_r(r)}{J} \quad (3.3)$$

where the Jacobian is

$$J = \left(1 + \frac{\Delta U}{r}\right)^2 \left(1 + \frac{\partial U(r)}{\partial r}\right),$$

and  $\Delta U(r) \equiv U(r) - U(0)$ , we make the large distance approximation, where we assume that any mode we analyse have a wavenumbers  $k$  satisfy  $kr \gg r$  throughout. Terms  $\frac{\Delta U(r)}{r}$  which are  $\sim \frac{\delta}{kr}$ , are ignored in comparison with  $\delta$ .

If  $\Phi$  drops as some power of  $r$ , then a Taylor expansion of  $\Phi(s)$  yields  $\Phi(r)$  plus negligible corrections terms.

From equation (8), we get the following equation,

$$\delta_s(s) = \frac{1 + \delta_r(r)}{J} - 1 = \frac{1 + \delta_r(r)}{\left(1 + \frac{\Delta U}{r}\right)^2 \left(1 + \frac{\partial U(r)}{\partial r}\right)} - 1 \quad (3.4)$$

For  $\frac{\Delta U(r)}{r} \rightarrow 0$  at a large scale, a third order term is given by Heavens et al. (1998)

$$\begin{aligned} \delta_s(s) &\simeq \frac{1 + \delta_r(r)}{\left(1 + \frac{\partial U(r)}{\partial r}\right)} - 1 = \delta_r(r) - \delta_r(r) \frac{\partial U(r)}{\partial r} + \left(\frac{\partial U(r)}{\partial r}\right)^2 - \frac{\partial U(r)}{\partial r} \\ &\quad + \delta_r(r) \left(\frac{\partial U(r)}{\partial r}\right)^2 - \left(\frac{\partial U(r)}{\partial r}\right)^3 \\ &= \delta_r(r) - U'(r) - \delta_r(r)U' + U'^2 + \delta_r(r)U'^2(r) - U'^3(r) \equiv F(r) \end{aligned} \quad (3.5)$$

To linear order, differences in the argument do not matter, but to the third order, they do. We expand to third order the density  $\delta_s(s) = F(r)$  function in function of the coordinate  $s$  in redshift space. We approximate to the third order a function  $F(r)$  in terms of values  $s$ ,

$$F(r) = F(s) - \Delta U F'(s)[1 - U'(s)] + \frac{1}{2} \Delta U^2(s) F''(s) \quad (3.6)$$

which gives the final expression for the redshift space overdensity in terms of real space overdensity, all evaluated at  $s$  position

$$\begin{aligned} \delta_s &= \delta_r - U' + U'^2 - \delta_r U' + \delta_r U'^2 - U'^3 - \Delta U \delta'_r + \\ &\quad \Delta U U'' - 3 \Delta U U' U'' + 2 \Delta U U'' \delta_r + \frac{1}{2} \Delta U^2 \delta''_r - \frac{1}{2} \Delta U^2 U'''. \end{aligned} \quad (3.7)$$

### B. Non linear bias

We make the Taylor expansion to the third order of  $\delta_r^g$  around the matter density  $\delta_r$

$$\delta_r^g = \langle g | \delta \rangle = \sum_{j=0}^{\infty} \frac{b_j}{j!} \delta_r^j = b_0 + b_1 \delta_r + \frac{b_2}{2!} \delta_r^2 + \frac{b_3}{3!} \delta_r^3. \quad (3.8)$$

In order to get the true value of the parameters  $b_i, i = 0, 1, 2, 3$ , in the simulation, we fitted parameters from GIF simulation for the density biasing of galactic halos versus mass in N-body simulation, see Fig. 1, (Dekel & Lahav 1998); we find that,  $b_0, b_1, b_2$  and  $b_3$ , are respectively 0.0041, 0.91,  $-0.0052$ , and 0.00157. The last term of a galaxy density in redshift space  $\delta_r^g$  is:

$$\begin{aligned} \delta_g^s &= b_0 + (b_1\delta_r - (1 + b_0)U') + \left[\frac{b_2}{2}\delta_r^2 + (1 + b_0)U'^2\right. \\ &\quad \left. - b_1\delta_r U' - b_1\Delta U\delta_r' + (1 + b_0)\Delta U U''\right] + \left[\frac{b_3}{6}\right. \\ \delta^3 r - \frac{b_2}{2}\delta_r^2 U' + b_1\delta_r U'^2 - U'^3 - b_2\Delta U\delta_r\delta_r' - 3\Delta U U' U'' & \\ \left. + \left[\frac{b_3}{6}\delta_r^3 - \frac{b_2}{2}U' + b_1\delta_r U'^2 - U'^3 - b_2\Delta U\delta_r\delta_r' - 3\Delta U U' U''\right] \right] &\equiv \delta_g^{s_0} + \delta_g^{s_1} + \delta_g^{s_2} + \delta_g^{s_3}. \end{aligned} \quad (3.9)$$

The Fourier transform of this may be taken in redshift space, by doing the transforms of simple products

$$\begin{aligned} (X_1)_k &= \frac{1}{(2\pi)^3} \int d^3 k_1 \delta^D(k - k_1) X_1 \\ (X_1 Y_2)_k &= \frac{1}{(2\pi)^3} \int d^3 k_1 d^3 k_2 \delta^D(k - k_1 - k_2) X_1 Y_2 \\ (X_1 Y_2 Z_3)_k &= \frac{1}{(2\pi)^6} \int d^3 k_1 d^3 k_2 d^3 k_3 \delta^D(k - k_1 - k_2 - k_3) X_1 Y_2 Z_3 \end{aligned} \quad (3.10)$$

where  $X_1, Y_2$  and  $Z_3$  are  $k_1, k_2,$  and  $k_3$  component of  $X_k,$  and  $\delta^D$  is the Dirac delta function. The third-order expansion of the fluid equations (Fry 1994) is detailed in Catelan and Moscardini (1994a,b), giving  $\delta_k$

$$\begin{aligned} \delta_k &= \epsilon_k + \frac{1}{(2\pi)^3} \int d^3 k_1 d^3 k_2 \delta^D(k - k_1 - k_2) J_s^{(2)}(k_1 - k_2) \epsilon_1 \epsilon_2 \\ &+ \frac{1}{(2\pi)^6} \int d^3 k_1 d^3 k_2 d^3 k_3 \delta^D(k - k_1 - k_2 - k_3) J_s^{(3)}(k_1 - k_2 - k_3) \epsilon_1 \epsilon_2 \epsilon_3 \end{aligned} \quad (3.11)$$

$\epsilon_k$  is the linear, real space Fourier coefficient of the density field  $\delta(r), \frac{\partial}{\partial r} \rightarrow ik\mu,$  where  $\mu = \frac{\hat{r}}{k}$  and  $\hat{r}$  is a unit vector from the observer to the galaxy, and the transform  $U$  is  $U_k = i\mu f \frac{\eta_k}{k},$  where  $-\eta_k$  is the transform of the velocity divergence.  $f \equiv \frac{d \ln D}{d \ln a} \simeq \Omega_0^{0.6},$  where  $D(a)$  is the growing mode amplitude, and  $a$  is the scale factor of the Universe. The corresponding expression for  $\eta_k$  involve replacing  $J$  by  $K.$  The function  $J$  and  $K$  are quoted for  $\Omega_0 = 1,$  as computed by Goroff et al. (1986), Catelan and Moscardini (1994a,b) as:

$$\begin{aligned} J_S^{(2)}(\mathbf{k}_1, \mathbf{k}_2) &= \frac{5}{7} + \frac{\mathbf{k}_1 \cdot \mathbf{k}_2}{2k_1 k_2} \left( \frac{k_1}{k_2} + \frac{k_2}{k_1} \right) + \frac{2}{7} \left( \frac{\mathbf{k}_1 \cdot \mathbf{k}_2}{k_1 k_2} \right)^2, \\ K_S^{(2)}(\mathbf{k}_1, \mathbf{k}_2) &= \frac{3}{7} + \frac{\mathbf{k}_1 \cdot \mathbf{k}_2}{2k_1 k_2} \left( \frac{k_1}{k_2} + \frac{k_2}{k_1} \right) + \frac{4}{7} \left( \frac{\mathbf{k}_1 \cdot \mathbf{k}_2}{k_1 k_2} \right)^2, \\ J^{(3)}(\mathbf{k}_1, \mathbf{k}_2, \mathbf{k}_3) &= J^{(2)}(\mathbf{k}_2, \mathbf{k}_3) \left[ \frac{1}{3} + \frac{1}{3} \frac{\mathbf{k}_1 \cdot (\mathbf{k}_2 + \mathbf{k}_3)}{(\mathbf{k}_2 + \mathbf{k}_3)^2} + \frac{4}{9} \frac{\mathbf{k} \cdot \mathbf{k}_1}{k_1^2} \frac{\mathbf{k} \cdot (\mathbf{k}_2 + \mathbf{k}_3)}{(\mathbf{k}_2 + \mathbf{k}_3)^2} \right] \\ &\quad - \frac{2}{9} \frac{\mathbf{k} \cdot \mathbf{k}_1}{k_1^2} \frac{\mathbf{k} \cdot (\mathbf{k}_2 + \mathbf{k}_3)}{(\mathbf{k}_2 + \mathbf{k}_3)^2} \frac{\mathbf{k}_3 \cdot (\mathbf{k}_2 + \mathbf{k}_3)}{k_3^2} + \frac{1}{9} \frac{\mathbf{k} \cdot \mathbf{k}_2}{k_2^2} \frac{\mathbf{k} \cdot \mathbf{k}_3}{k_3^2} \\ K^{(3)}(\mathbf{k}_1, \mathbf{k}_2, \mathbf{k}_3) &= 3J^{(3)}(\mathbf{k}_1, \mathbf{k}_2, \mathbf{k}_3) - \frac{\mathbf{k} \cdot \mathbf{k}_1}{k_1^2} J^{(2)}(\mathbf{k}_2, \mathbf{k}_3) - \frac{\mathbf{k} \cdot (\mathbf{k}_1 + \mathbf{k}_2)}{(\mathbf{k}_1 + \mathbf{k}_2)^2} K^{(2)}(\mathbf{k}_1, \mathbf{k}_2), \end{aligned}$$

with  $\mathbf{k} = \mathbf{k}_1 + \mathbf{k}_2 + \mathbf{k}_3$  in the last two expressions. Here we can give the corresponding Fourier transforms for each density's part at third order;

$$\begin{aligned}
 \delta_r^3 &\longrightarrow \epsilon_1 \epsilon_2 \epsilon_3 \\
 -\frac{1}{2} \delta_r^2 U' &\longrightarrow \left[ \frac{1}{2} f \mu_3^2 + \frac{1}{2} f \mu_1 \mu_2 \frac{k_2}{k_1} + \frac{1}{2} f \mu_1 \mu_3 \frac{k_1}{k_3} \right] \epsilon_1 \epsilon_2 \epsilon_3 \\
 \Delta U \delta_r \delta_r' &\longrightarrow [J^{(2)}(\mathbf{k}_2, \mathbf{k}_3)] \epsilon_1 \epsilon_2 \epsilon_3 \\
 -U^3 &\longrightarrow \left[ f^3 \mu_1^2 \mu_2^2 \mu_3^2 + 3 f^3 \mu_1 \mu_2^2 \mu_3^3 \frac{k_3}{k_1} + \frac{1}{2} f^3 \mu_1 \mu_2 \mu_3^4 \frac{k_3^2}{k_1 k_2} \right] \epsilon_1 \epsilon_2 \epsilon_3 \\
 \delta_r U'^2 &\longrightarrow f^2 \left[ \mu_2^2 \mu_3^2 + 2 \mu_1 \mu_2 \mu_3^2 \frac{k_1}{k_2} + \mu_2 \mu_3^3 \frac{k_3}{k_2} + \frac{1}{2} \mu_1^2 \mu_2 \mu_3 \frac{k_1^2}{k_2 k_3} \right] \epsilon_1 \epsilon_2 \epsilon_3 \\
 2 \delta_r' \Delta U U' &\longrightarrow J^{(2)}(\mathbf{k}_2 \mathbf{k}_3) f \left[ \mu_1^2 + \mu_{2+3} \frac{k_{2+3}}{k_1} \right] \epsilon_1 \epsilon_2 \epsilon_3 \\
 \delta_r \Delta U U'' &\longrightarrow f K^2(\mathbf{k}_2, \mathbf{k}_3) \left[ \mu_{2+3}^2 + \mu_1 \mu_{2+3} \frac{k_1}{k_{2+3}} \right] \epsilon_1 \epsilon_2 \epsilon_3 \\
 \frac{1}{2} \delta_r'' (\Delta U)^2 &\longrightarrow [J^{(3)}(\mathbf{k}_1, \mathbf{k}_2, \mathbf{k}_3)] \epsilon_1 \epsilon_2 \epsilon_3 \\
 -3 \Delta U U' U'' &\longrightarrow f^2 K^2(\mathbf{k}_2, \mathbf{k}_3) \left[ 2 \mu_1^2 \mu_{2+3}^2 + \mu_1 \mu_{2+3}^3 \frac{k_{2+3}}{k_1} \right] \epsilon_1 \epsilon_2 \epsilon_3 \\
 -\frac{1}{2} (\Delta U)^2 U''' &\longrightarrow [f \mu^2 K^3(\mathbf{k}_1, \mathbf{k}_2, \mathbf{k}_3)] \epsilon_1 \epsilon_2 \epsilon_3 \tag{3.12}
 \end{aligned}$$

where  $\epsilon_1, \epsilon_2$  and  $\epsilon_3$  are respectively the linear, real space Fourier coefficient of the density field  $\delta_1(r), \delta_2(r)$  and  $\delta_3(r)$ , such that  $\epsilon_1 = \delta_{\mathbf{k}_1, g}^{(1)}, \epsilon_2 = \delta_{\mathbf{k}_2, g}^{(1)}$  and  $\epsilon_3 = \delta_{\mathbf{k}_3, g}^{(1)}$ .

The fourier transform of density in redshidt space  $\delta_g^s$  is

$$\begin{aligned}
 (\delta_g^s)^2 &= (1 + b_0) F_s^{(1)}(k) \delta_{\mathbf{k}_1, g}^{(1)} + \frac{1}{(2\pi)^3} \int d^3 k_1 d^3 k_2 \delta^D(k - k_1 - k_2) F_s^{(2)}(k_1, k_2) \delta_{\mathbf{k}_1, g}^{(1)} + \delta_{\mathbf{k}_2, g}^{(2)} \\
 &\frac{1}{(2\pi)^6} \int d^3 k_1 d^3 k_2 d^3 k_3 \delta^D(k - k_1 - k_2 - k_3) F_s^{(3)}(k_1, k_2, k_3) \delta_{\mathbf{k}_1, g}^{(1)} \delta_{\mathbf{k}_2, g}^{(2)} \delta_{\mathbf{k}_3, g}^{(3)}
 \end{aligned}$$

where

$$\begin{aligned}
 F_s^{(1)}(k) &= b_1 + (1 + b_0) f \mu^2 \\
 F_s^{(2)}(\mathbf{k}_1, \mathbf{k}_2) &= b_1 J_s^{(2)}(\mathbf{k}_1, \mathbf{k}_2) + (1 + b_0) f^2 K_s^{(2)}(\mathbf{k}_1, \mathbf{k}_2) + \frac{b_2}{2} \\
 &+ \frac{b_1 f}{2} \left[ \mu_1^2 + \mu_2^2 + \mu_1 \mu_2 \left( \frac{k_1}{k_2} + \frac{k_2}{k_1} \right) \right] + (1 + b_0) f^2 \left[ \mu_1^2 \mu_2^2 + \frac{\mu_1 \mu_2}{2} \left( \mu_1^2 \frac{k_1}{k_2} + \mu_2^2 \frac{k_2}{k_1} \right) \right] \\
 F_s^{(3)}(\mathbf{k}_1, \mathbf{k}_2, \mathbf{k}_3) &= b_1 J^{(3)}(\mathbf{k}_1, \mathbf{k}_2, \mathbf{k}_3) + f \mu^2 K^{(3)}(\mathbf{k}_1, \mathbf{k}_2, \mathbf{k}_3) + \frac{b_2}{2} f \mu_3^2 + \frac{b_3}{6} \\
 &+ \frac{b_2}{2} f \mu_1 \mu_2 \frac{k_2}{k_1} + \frac{b_2}{2} f \mu_1 \mu_3 \frac{k_3}{k_1} + b_1 f^2 \mu_2^2 \mu_3^2 + 2 b_1 f^2 \mu_1 \mu_2 \mu_3^3 \frac{k_1}{k_2} + b_1 f^2 \mu_2 \mu_3^3 \frac{k_3}{k_2} + \frac{b_1}{2} f^2 \mu_1^2 \mu_2 \mu_3 \frac{k_1^2}{k_2 k_3} \\
 &+ f^3 \mu_1^2 \mu_2^2 \mu_3^2 + 3 f^3 \mu_1 \mu_2^2 \mu_3^3 \frac{k_3}{k_1} + \frac{1}{2} f^3 \mu_1 \mu_2 \mu_3^4 \frac{k_3^2}{k_1 k_2} + J^{(2)}(\mathbf{k}_2, \mathbf{k}_3) \left( b_2 + b_1 f \mu_1^2 + b_1 f \mu_1 \mu_{2+3} \frac{k_{2+3}}{k_1} \right) \\
 &+ K^{(2)}(\mathbf{k}_2, \mathbf{k}_3) \left( b_1 f \mu_{2+3}^2 + b_1 f \mu_1 \mu_{2+3} \frac{k_1}{k_{2+3}} + 2 f^2 \mu_1^2 \mu_{2+3}^2 + f^2 \mu_1 \mu_{2+3}^3 \frac{k_{2+3}}{k_1} + f^2 \mu_1^3 \mu_{2+3} \frac{k_1}{k_{2+3}} \right). \tag{3.13}
 \end{aligned}$$

If we neglect the  $b_0$  term in equation (14), required to ensure that  $\langle \delta_r^2 \rangle = 0$ , this is the Heavens case, Heavens et al. (1998); but in our case we also take this term into consideration.

After doing all the calculations, the transform of the third order biased, redshift-space density fields becomes as,

$$\begin{aligned} \delta_s^g(k) &= F_s^1(k)\epsilon_k + \frac{1}{(2\pi)^3} \int d^3k_1 d^3k_2 \delta^D(k - k_1 - k_2) J_s^{(2)}(k_1 - k_2) \epsilon_1 \epsilon_2 \\ &+ \frac{1}{(2\pi)^6} \int d^3k_1 d^3k_2 d^3k_3 \delta^D(k - k_1 - k_2 - k_3) J_s^{(3)}(k_1 - k_2 - k_3) \epsilon_1 \epsilon_2 \epsilon_3 \end{aligned} \quad (3.14)$$

The redshift space power spectrum  $P_s^g(\mathbf{k})$  is defined by

$$\langle \delta_{s k_1}^g \delta_{s k_2}^g \rangle = (2\pi)^3 P_s^g(k_1) \delta^D(\mathbf{k}_1, \mathbf{k}_2) \quad (3.15)$$

and the real-space mass linear power spectrum  $P_{11}(\mathbf{k})$  is defined similarly by

$$\langle \epsilon_1 \epsilon_2 \rangle = (2\pi)^3 P_{11}(\mathbf{k}_1) \delta^D(\mathbf{k}_1 + \mathbf{k}_2) \quad (3.16)$$

The Gaussian nature of the initial fluctuation implies, by Wick's theorem that  $\langle \epsilon_1 \epsilon_2 \epsilon_3 \rangle = 0$  and  $\langle \epsilon_1 \epsilon_2 \epsilon_3 \epsilon_4 \rangle = \langle \epsilon_1 \epsilon_2 \rangle \langle \epsilon_3 \epsilon_4 \rangle$  plus cyclic permutation, thus, the final formula of power spectrum for galaxies in redshift space is as

$$\begin{aligned} P_s^g(\mathbf{k}) &\equiv P_g^{s11} + P_g^{s22} + P_g^{s13} = [1 + (1 + b_0)\beta\mu^2]^2 b_1^2 P_{11}^k + 2 \int \frac{d^3q}{(2\pi)^3} P_{11}(q) P_{11}(|\mathbf{k} - q|) \\ &[F_s^{(2)}(q, \mathbf{k} - q)]^2 + 6(1 + \beta\mu^2) b_1 P_{11}(\mathbf{k}) \int \frac{d^3q}{(2\pi)^3} P_{11}(q) F_s^{(3)}(q, -q, \mathbf{k}) \end{aligned} \quad (3.17)$$

and the non-linear power spectrum for matter in real and redshift space are respectively given by this two formula

$$\begin{aligned} P_\delta^r(k)_{NL} &= b_1^2 P_{11}(k) + 2 \int \frac{d^3q}{(2\pi)^3} P_{11}(q) P(|\mathbf{k} - q|) [F_s^2(q, \mathbf{k} - q)]^2 \\ &+ 6b_1^2 P_{11}(k) \int \frac{d^3q}{(2\pi)^3} P_{11}(q) F_s^{(3)}(q, -q, \mathbf{k}) \end{aligned} \quad (3.18)$$

and

$$\begin{aligned} P_\delta^s(k)_{NL} &= (1 + \beta\mu^2) P_{11}(k) [(1 + \beta\mu^2) + 2 \int \frac{d^3q}{(2\pi)^3} P_{11}(q) P(|\mathbf{k} - q|) [F_s^2(q, \mathbf{k} - q)]^2 \\ &+ 6 \int \frac{d^3q}{(2\pi)^3} P_{11}(q) F_s^{(3)}(q, -q, \mathbf{k})] \end{aligned}$$

The different power spectra showed in non-linear effect, redshift distortion and non-linear bias are founded yielded as follows:

The first real power spectrum in the linear case  $P_\delta^r(k)_L$  is obtained by fitting function for ( $\Lambda$  CDM), while the second power spectrum  $P_\delta^r(k)_{NL}$  is computed by putting  $f(\Omega) = 0$  ie;  $\beta = 0$ , and  $b_2 = b_3 = 0$ , but  $b_1 \neq 0$ . For  $b_1 = 1$  and  $b_i = 0; i \neq 1$  leads to get  $\delta_g = \delta_m$ , then the power  $P_\delta^s(k)_{NL}$  goes to be the power spectra  $P_\delta^s(k)_{NL}$ . For this last two figures, to get the non-linear bias and non-linear dynamics for the galaxies in redshift space, we applied this following method; the first is to see the non-linear effects from  $P_\delta^r(k)_L$  to  $P_\delta^r(k)_{NL}$ , the redshift distortion from  $P_\delta^r(k)_{NL}$  to  $P_\delta^s(k)_{NL}$ , and finally to see the non-linear bias effect between  $P_\delta^s(k)_{NL}$  and  $P_g^s(k)_{NL}$  in the redshift space. We can represent the evolving complexity of different power spectrum as:

$$P_\delta^r(k)_L \longrightarrow P_\delta^r(k)_{NL} \longrightarrow P_\delta^s(k)_{NL} \longrightarrow P_g^s(k)_{NL}.$$

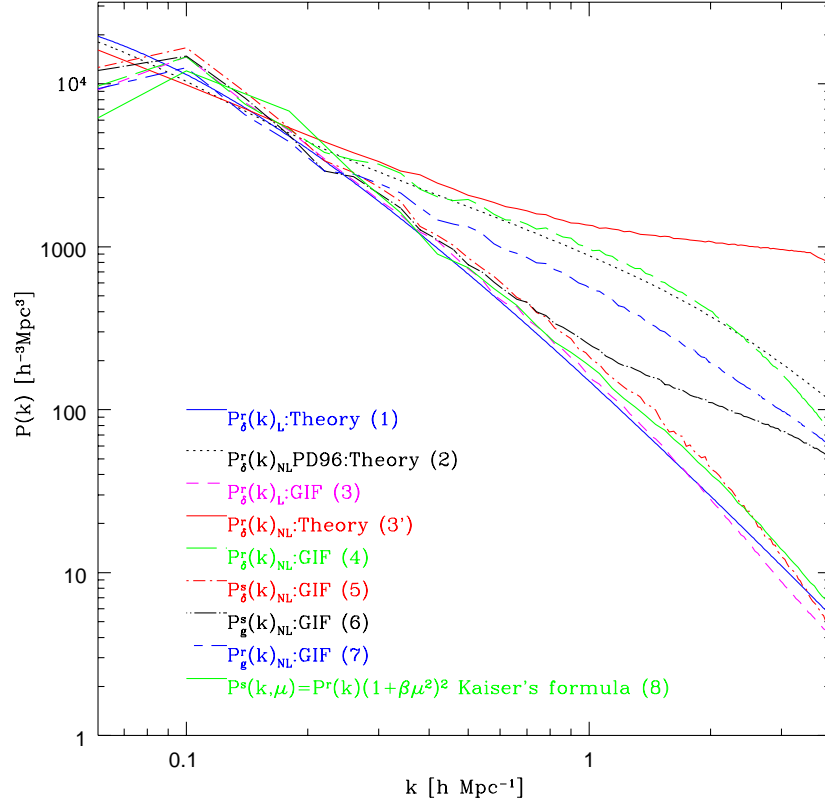


FIG. 2. Different power spectrum form GIF simulation analysis compared with the theory cases. The blue solid line (1) is the matter linear power spectrum in the real space while the black dotted line (2) is the real matter non linear power spectrum calculated by Peacock and Dodds (P&D 96). The following plot are all calculated from the GIF data simulation. The green solid line showed the Kaiser's formula power spectrum for galaxies in redshift space line(8). The magenta dashed line (3) is the matter linear power spectrum in real space while the non linear real power spectrum is given by the green dashed line (4). The red solid line present the non-linear power spectrum for matter line(3'). The non-linear power spectrum for the matter and galaxies in redshift space from the simulation are respectively characterized by the red and black dotted dashed line (5 & 6). The dashed blue line (7) is the galaxy non-linear real power spectrum. For more details see text.

The theoretical and simulation real power spectrum for matter in the linear regime  $P_{\delta}^r(k)_L$  are in agreement with the Kaiser's formula, which implies the validity of our theoretical prediction with this formula. Also, we have the theoretical and simulation analysis of data for matter power spectrum in the non-linear regime  $P_{\delta}^r(k)_{NL}$  are similar to Peacock prediction fitting which is working well in this regime. The non-linear evolution prediction by the fitting formula of Peacock & Dodds (1996, hereafter PD96) is given as:

$\Delta_{NL}^2(k_{NL}, z) = f_{NL}[\Delta_L^2(k_L)]$ , where  $\Delta_k^2 = \frac{dp(k, z)}{dlnk}$  and subscripts  $L$  and  $NL$  denote the linear and non-linear quantities, respectively. The analytical expression of  $f_{NL}$  depends on five fitting parameters (see § 3.3 in PD96) obtained by fitting the power spectra of the scale free N-body simulation.

For the matter in redshift space we found that the GIF data analysis for the power spectrum  $P_{\delta}^r(k)_L$  in the linear regime agrees with the Kaiser's formula  $P^s(k, \mu) = P^r(1 + \beta\mu^2)^2$  at large scale (ie,  $k$  small), but at small scale  $k$  (ie,  $k$  large) which this formula is not working, the results are roughly different. Here we are showed the validity of our theory with the Kaiser formula which is working just in the linear regime.

The simulation results corresponds to the non-linear effect in real space between the power spec-

trum for matter  $P_{\delta}^r(k)_{NL}$  and power spectrum for galaxies  $P_g^r(k)_{NL}$  started at wavenumbers  $k \simeq 0.2h \text{ Mpc}^{-1}$ .

The redshift distortion effect is remarked also from the simulation between the galaxies in real and redshift space. We can see this effect from the difference in the non-linear regime between the power spectrum in real space  $P_g^r(k)_{NL}$  and the power spectrum in redshift space  $P_g^s(k)_{NL}$ . This effect appear at scale  $k \simeq 0.25h \text{ Mpc}^{-1}$  and becomes more important at large scale.

For the simulation power spectrum in real and redshift space, we can see the difference between them, such that the  $P_g^s(k)_{NL}$  is lower than  $P_g^r(k)_{NL}$  in real space which is in agreement with the result found at epoch  $z=0$  in Figure, 4 in Gottlöber et al. (1998), but in this case he showed his results with different circular velocities for galaxies, and also this results roughly similar to Figure 1 in Andrey et al. (1999).

We can see also from the data analysis that  $P_{\delta}^s(k)_{NL}$  is slower than the galaxies power spectrum  $P_g^s(k)_{NL}$ . Although the scale of non-linearity (wavenumber) of an upward inflection of  $P_g^s(k)_{NL}$  is seen clearly in and approximately matches the corresponding scale in  $P_{\delta}^s(k)_{NL}$  at epoch ( $z=0$ ), the shapes of the galaxies (halo) and matter power spectra are quite different. This difference means that the bias of galaxies distribution is scale dependent. A similar conclusion has been reached by many authors from comparisons of galaxies and matter two point correlation function (e.g, Bagla 1998; Colin et al. 1998; Katz, Hernquist & Weinberg 1998).

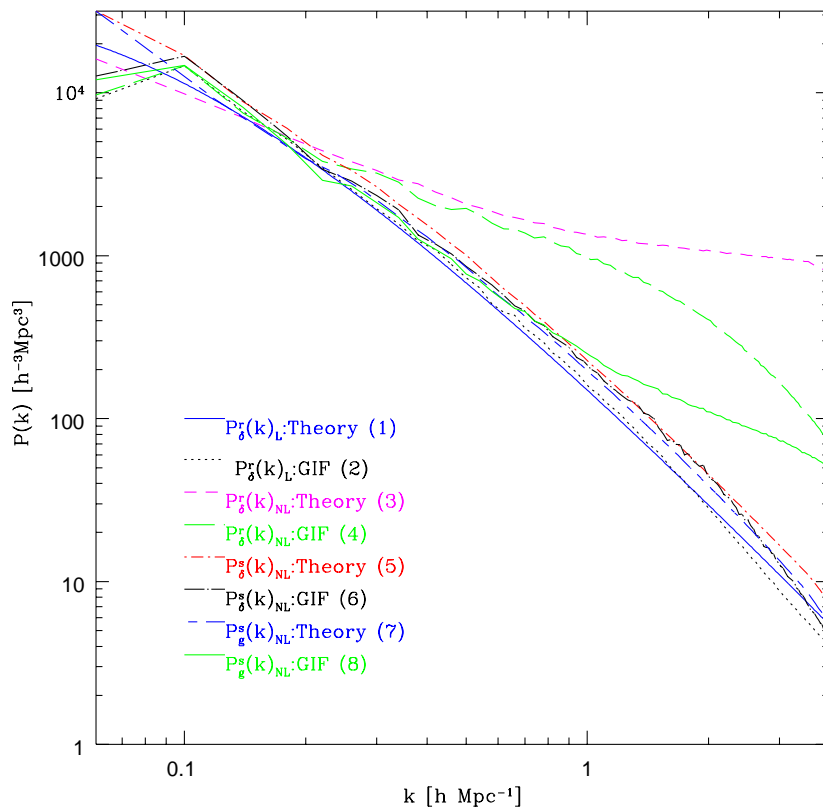


FIG. 3. Different power spectrum calculated from the theory compared with GIF simulation. The plot are given par odd numbers are the theoretical calculation, such as: The blue solid line (1) correspond to the matter linear power spectrum in real space while the magenta dashed line (3) and the red dashed line (5) are respectively the non-linear matter power spectrum in real and redshift space. The dashed blue line (7) is the non-linear galaxies power spectrum in redshift space. The even numbers of the plots correspond to the GIF's data analysis where the dotted line (2) and green-dashed line (4) are the linear and non-linear matter power spectrum in real space respectively, while the black dashed-line (6) and the solid green line (8) are the matter and galaxies non-linear power spectrum in redshift space respectively. For more details see text.

For more details in Figure 3, we can discuss here how much difference we have (or is there an agreement or not) with the GIF's data simulation analyzed and the theory prediction.

The non-linear effect for power spectrum of matter theoretically  $P_{\delta}^r(k)_{NL}$  and simulation data analyzed here are started respectively at wavenumbers  $k \simeq 0.15 \text{ hMpc}^{-1}$  and  $k \simeq 0.17 \text{ hMpc}^{-1}$  which means an agreement between this two quantities, while the redshift distortion effect between the power spectrum for the matter in real space  $P_{\delta}^r(k)_{NL}$  and redshift space  $P_{\delta}^s(k)_{NL}$  are started for theory and simulation respectively at  $k \simeq 0.22 \text{ hMpc}^{-1}$  and  $k \simeq 0.20 \text{ hMpc}^{-1}$ . In both cases these last two power spectra, the one in real space is lower than the one in redshift space, which agrees with the result at  $z=0$  in Figure 3, in Gottlöber et al. (1998), and Figure 1 in Andrey et al. (1999).

The non-linear bias effect in redshift space between the mass power spectrum  $P_{\delta}^s(k)_{NL}$  and galaxies power spectrum in redshift space  $P_g^s(k)_{NL}$  demonstrated in the theory and simulation respectively at  $k \simeq 0.01 \text{ hMpc}^{-1}$  and  $k \simeq 0.8 \text{ hMpc}^{-1}$ . The two quantities in theory and simulation are started at different scales. It means that the theoretical prediction applied here is not well working against the simulation analysis. This difference is due to the theory approximation, because we have just approximated to the third order of the galaxy density perturbation equation(13) which implies that if we take higher order of perturbation, this two quantities becomes in agreement each to other.

We remarked for the theory and the simulation analysis for galaxies in redshift space, that we found at small scale (non-linear regime) from the range  $k \leq 0.7 \text{ hMpc}^{-1}$  that the result are not very well agrees in this range, we explains this difference is due to the non-linear bias such that the formula (13) is not exact, is just the third order in Taylor expansion, and we expected that each time when we increase the order in this formula the theory result becomes more closed and well agree with the simulation result, and this difference disappear then  $P_g^s(k)_{NL}$  becomes very similar to both theory and simulation.

#### IV. CONCLUSION AND DISCUSSION

For our simulation analysis, we investigated the measurement of the  $\beta$  parameter in the redshift space from the anisotropy of the redshift space power spectrum using the approach of the quadrupole to monopole ratio. We took the line-of-sight direction to be a Cartesian axis of the simulation cube, implicitly assuming that the whole simulation volume is far away to satisfy the distant observer approximation.

We presented the results from a study of the bias of dark matter and galaxies distribution in real and redshift space at large scale, high resolution simulation assuming a flat, CDM model with a cosmological constant. The following conclusions can be drawn from the results presented in this paper. Figure 1, represents the function  $\beta(\lambda)$  obtained from solving for  $\beta$  in equations (4) and (5) respectively, where  $\lambda = \frac{2\pi}{k}$ .

We have presented a calculation of the anisotropy in s-space power spectrum using the quadrupole to monopole power spectrum to estimated the  $\beta$  parameter. The decline of this ratio on large scale is due to the non-linear effects, coherent effect and peculiar velocities. Also, in this paper we showed that the different power spectra consistent in the linear and non linear regime, i.e.: at small and large scales both in the theory and in the analysis of GIF simulation data. In our studies, we found good agreement between the predictions of the theory and the data from the GIF N-body simulation.

At  $z=0$ , the real space power spectrum of dark matter shows a clear excess over the linear power spectrum due to non-linear clustering. The corresponding dark matter power spectrum in redshift space follows almost exactly the linear power spectrum of dark matter.

The comparison between our results for power spectrum for the matter and galaxies in real and redshift space at  $z=0$  with the Figures 3 and 4 in Gottlöber et al, (1998) shows that there is very agreement. Here we can see the bias with these two quantities such that in real space the power spectrum of galaxies (halo) and matter are very different.

We showed that the theory we applied here is agrees well with the data of GIF N-body simulation.

For the different case, different regime and different space, there is an agreement between each of the two spectra which gives a certain confidence to the theory applied.

The evolution of the power spectrum of the galaxies distribution is significantly slower than the evolution of the matter power spectrum (both linear and non-linear) scales. The galaxies and matter power spectra also have significantly different shapes. The differences in shape imply scale dependent bias of the galaxies distribution.

At  $z = 0$  the halo power spectrum in our simulation analysis matches the observed power spectrum of the APM galaxies well.

Despite the difference in shape, the power spectra of both matter and galaxies exhibit a distinct “inflection point” at approximately the same wavenumbers, corresponding to the scale of non-linearity (ie., the scale at which the power spectra begin to deviate significantly from the linear power spectrum). The inflection scale is  $k \simeq 0.25 h Mpc^{-1}$  and very close to the inflection observed in the power spectrum of the APM galaxies (Gaztañaga & Baugh 1998); therefore, we interpret the inflection in the APM power spectrum as the present-day scale of non-linearity  $k_{NL}$ . We should note that the distinct inflection point can be seen only in the real space power spectrum; the non-linear amplitude of the redshift-space power spectrum is strongly suppressed and the inflection in the power spectrum of both matter and galaxies is smoothed out (see Figs. 3 & 4 in Gottlöber et al. 1998).

The analytic fitting formula of Peacock & Dodds (1996), with only minor tuning, provides an excellent match to both the shape and evolution rate of the matter power spectrum in our simulation analysis. The latter probes deep into the non-linear regime, down to wave numbers of ( $\sim 0.2 h Mpc^{-1}$ ) at ( $z=0$ ); we find that clustering of dark matter in the highly non-linear regime in the simulation is approximately stationary (stable clustering). This result of this paper implies that detailed modeling of the small-scale galaxy clustering requires a good understanding of galaxy evolution in clusters.

The author would like to thank A. Dekel, E. Rabinovici and M. Virasoro and ICTP for help. He also thanks Cristiano Porciani and Amiram Eldar for fruitful discussions.

## V. REFERENCES

- 
- A. F. Heavens, S. Matarrese and L. Verde, 1998 MNRAS 301, 797H  
 Andreas A, Berlind, Vijay K. Narayanan, and David H. Weinberg, 2001, ApJ, 549, 688  
 Andrey, V. et al, 1999 ApJ, 520, 437K  
 Bagla, J. S. 1998, MNRAS, 299, 417  
 J. A., Peacock, S. J. Dodds, 1996 MNRAS, 280L, 19P  
 Catelan P., Moscardini L., 1994a, ApJ, 426, 14  
 Catelan P., Moscardini L., 1994b, ApJ, 436, 5  
 Cole, S., Fisher, K. B., & Weinberg, D. H. 1995, MNRAS, 275, 515  
 Colin, P., Klupin, A. A., Kravtsov, A. V., Khokhlov, A. M., 1998, ApJ, 523 (1999) 32  
 Dekel, A, Lahav, O, 1999 ApJ, 520, 24D, (astro-ph/9806193)  
 Eke, V. R., Cole, S., & Frenk, C. S. 1996, MNRAS, 282, 263  
 Evrad, A. E. 1997, ApJ, 292, 289

- Falco, E. E., Shapiro, I. I., Moustakas, L. A., Davis, M. 1997, ApJ, 484, 70  
Fisher, K. B., & Nusser, A. 1996, MNRAS, 279, L1  
Fry J. N., 1984, ApJ, 279, 499  
Gaztañaga, E., & Baugh, C.M. 1998, MNRAS, 294, 229  
Goroff M. H., Grindstein B., Rey S. J., Wise B., 1986, ApJ, 311, 6  
Hatton, S. J., & Cole, S. 1999, MNRAS, 310, 113  
Kaiser N., 1987, MNRAS, 227,1  
Katz, N., Hernquist, L. & Weinberg, D. H. 1999, ApJ, 523, (1999),463  
Madore, B. F. et al. 1999, ApJ,515, (1999) 29  
McGill C., 1990, MNRAS, 242,428  
S. Gottlöber, A. A. Klypin, A. V. Kravtsov, ASP Conference Series Vol. 176, 1999, "Observational Cosmology: The Development of Galaxy Systems", eds.: G. Giuricin, M. Mezzetti, P. Salucci, p. 418  
Peebles, P. J. E. 1980, The Large Scale Structure of the Universe (Princeton: Princeton Univ. Press)  
Perlmutter, S., et al. 1999, ApJ, 517 (1999) 565-586  
Salaris, M., & Cassisi, S. 1998, MNRAS, 298, 166